

Fully Constrained Least Squares for Antarctic Sea Ice Concentration Estimation Utilizing Passive Microwave Data

Tingting Liu, *Member, IEEE*, Yanxia Liu, Xin Huang, *Senior Member, IEEE*, and Zemin Wang

Abstract—To improve the accuracy of the traditional NASA Team (NT) sea ice concentration (SIC) algorithm, a new SIC estimation method is proposed by combining the NT algorithm and a numerical optimization technique with Special Sensor Microwave/Imager (SSM/I) data. In this method, the noise is taken into consideration to improve the SIC estimation equation, and then, the least squares method is used to further optimize the estimation results from the improved equation. Validation was performed using a comparison between the results from the SSM/I-based SICs (the proposed method, the NT algorithm, and the bootstrap algorithm) and *in situ* data. The quantitative results show that the proposed method generates a more accurate SIC with smaller bias ($-3.2\text{--}2.8$) and root-mean-square error (7.7–18.4) than the other two algorithms.

Index Terms—Antarctic Sea Ice Processes and Climate (ASPeCt), fully constrained least squares (FCLS), NASA Team (NT) algorithm, sea ice concentration (SIC).

I. INTRODUCTION

SEA ice concentration (SIC) is an important indicator of polar sea ice change and global climate change [1], [2]. In general, SIC is estimated utilizing passive microwave data, which are effective due to the daily revisit, the relatively low sensitivity to atmospheric water content and clouds, and the large contrast in emissivity between open water (OW) and sea ice. Various passive microwave-data-based SIC estimation methods have been proposed based on the difference of the multichannel brightness temperature (BT) distribution of different surface cover types (sea ice or OW) [3]–[5]. In terms of the different frequencies, these methods can be divided into two groups: 1) the low-frequency (19 and 37 GHz) data-based SIC estimation methods, such as the bootstrap algorithm [6], the NASA Team (NT) algorithm [7], and the CalVal algorithm [8];

Manuscript received June 2, 2015; revised July 25, 2015 and August 16, 2015; accepted August 19, 2015. Date of publication September 7, 2015; date of current version October 27, 2015. This work was supported in part by the National Natural Science Foundation of China under Grants 41206177 and 91338111, by the National High Technology Research and Development Program of China (863 Program) under Grants 2013AA12A301 and 2012AA12A304, and by the fund of the Key Laboratory of Global Change and Marine-Atmospheric Chemistry, State Oceanographic Administration, under Grant GCMAC1405.

T. Liu, Y. Liu, and Z. Wang are with the Chinese Antarctic Center of Surveying and Mapping, Wuhan University, Wuhan 430079, China (e-mail: tliu23@whu.edu.cn; liuyanxia123456skk@163.com; zmwang@whu.edu.cn).

X. Huang is with the State Key Laboratory of Information Engineering in Surveying, Mapping, and Remote Sensing, Wuhan University, Wuhan 430079, China (e-mail: huang_whu@163.com).

Color versions of one or more of the figures in this paper are available online at <http://ieeexplore.ieee.org>.

Digital Object Identifier 10.1109/LGRS.2015.2471849

and 2) the high-frequency (85 GHz) data-based SIC estimation methods, such as the ARTIST (Arctic Radiation and Turbulence Interaction STudy) Sea Ice (ASI) algorithm [9], the NT 2 algorithm [10], and the Near 90 GHz algorithm [11]. Although data of high frequencies have a fine resolution, they are more sensitive to atmospheric effects and the surface layer over OW due to their lower atmospheric transparency.

The well-known NT algorithm, which is based on the ratios of the BTs and the proposed SIC estimation equation, is capable of simultaneously estimating the SICs of three surface types [first year ice (FYI), multiyear ice (MYI), and OW]. In some studies [3]–[5], it was found that the NT algorithm often underestimates the SIC due to its sensitivity to cloud liquid water, atmospheric water vapor, the influence of sea surface roughness caused by wind, and many other factors. SIC estimation is also subject to the computational process. For example, the SIC estimation can be optimized through numerical calculation; however, the optimization issue has been largely ignored in previous studies. Therefore, in this letter, numerical optimization is introduced into the estimation to find the best matching SICs. Specifically, fully constrained least squares (FCLS) is used to build an optimization equation to estimate the SICs for multiple ice types.

The remainder of this letter is organized as follows. The experimental data and study area are described in Section II. The proposed FCLS-based SIC estimation approach is described in Section III, followed by the experimental results in Section IV. Section V concludes the study.

II. DATA SOURCES

A. SSM/I Radiometer Data

The Special Sensor Microwave/Imager (SSM/I) is a passive microwave radiometer, which is flown onboard the U.S. Air Force Defense Meteorological Satellite Program Block 5D-2 satellites. There are seven channels that measure BT at 19, 37, and 85 GHz with dual polarization and at 22 GHz with vertical polarization. The sampling distance at 19, 22, and 37 GHz is 25 km, and that at 85 GHz is 12.5 km. In this letter, the 19V, 19H, and 37V channels from the level-2 swath data were used.

B. ASPeCt Data Set

In this letter, the SIC *in situ* data were obtained from the Antarctic Sea Ice Processes and Climate (ASPeCt) program, which was established by the Scientific Committee on Antarctic

TABLE I
ICE TYPES USED IN THE ASPECT DATA SET

Ice type classes	Code	Ice type classes	Code
New ice	10,11,12,20	Pancakes	30
Young grey ice	40	Young grey-white ice	50
First year ice	60, 70, 80	Multi-year ice	85
Brash	90	Fast ice	95

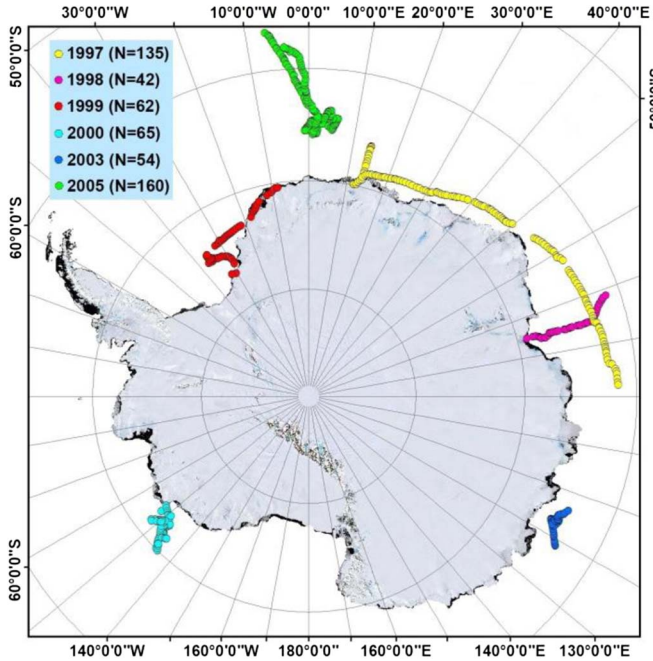


Fig. 1. ASPeCt experimental data distribution map. The dots, which are colored by year, indicate the corresponding location of each observation. N is the number of observed records in the corresponding year.

Research in 1997 [12]. These data are typically recorded every hour through ship-based observations. Total SIC and the SICs for different ice types used here are recorded in these data. In this data set, the ice types were classified according to thickness (see Table I).

For the NT algorithm and the proposed method, sea ice was divided into two types: FYI and MYI. To validate the SICs from different ice types, the SIC record in the ASPeCt data set was divided into two classes: 1) MYI (code “85” in Table I) and 2) FYI (all other codes in Table I).

The *in situ* data used in the experimental studies are plotted in Fig. 1. The total number of records amounted to 1080. However, some observations were located within a single pixel, considering the coarse resolution of passive microwave data. Therefore, their mean value was used in the analysis. Finally, a total of 518 records were used for the validation and comparison.

III. METHODOLOGY

Here, the proposed method is first presented, and some aspects of the method are further discussed.

A. Proposed Method

The basic equation of the NT-based SIC estimation is

$$T_B = T_{BW}C_W + T_{BFYI}C_{FYI} + T_{BMYI}C_{MYI} \quad (1)$$

TABLE II
BT (KELVIN) OF THE TIE POINTS FOR EACH SURFACE COVER TYPE IN THE DIFFERENT CHANNELS

Channels	Surface cover type		
	OW	FYI	MYI
19.4H	100.30	237.80	193.70
19.4V	176.60	249.80	221.60
37V	200.50	243.30	190.30
PR	0.28	0.02	0.07
GR	0.06	-0.01	-0.08

where T_B is the observed BT of each pixel from the satellite image. T_{BW} , T_{BFYI} , and T_{BMYI} , representing the BT of pure OW, FYI, and MYI, respectively, are the prior knowledge derived from the tie points. C_W , C_{FYI} , and C_{MYI} , which need to be obtained, represent the corresponding SICs of each surface cover type.

It should be noted that the observed BT can be expressed as the combination of the three dominant ocean surface cover types. In a real situation, certain factors that may result in noise n in (1) should be taken into consideration to further improve the estimation accuracy. For example, the sensor resolution can lead to discrepancies in BT values between the images and the corresponding tie points, and attenuation associated with surface radiation transfer can lead to T_B changes. Therefore, T_B can be reformulated as follows:

$$T_B = T_{BW}C_W + T_{BFYI}C_{FYI} + T_{BMYI}C_{MYI} + n. \quad (2)$$

For multichannel passive microwave data, (2) can be rewritten in a compact matrix form as

$$\mathbf{T} = \mathbf{M}\boldsymbol{\alpha} + \mathbf{n} \quad (3)$$

where \mathbf{T} is a $t \times 1$ column vector, denoted as the multi-channel passive microwave data of a pixel, and t is the total number of channels. \mathbf{M} is a $t \times 3$ matrix denoted by $[T_{BW} \ T_{BFYI} \ T_{BMYI}]$, where T_{BW} , T_{BFYI} , and T_{BMYI} are $t \times 1$ vectors, respectively, which are represented by the corresponding BTs from the observation-based tie points in each channel. $\boldsymbol{\alpha} = (\alpha_1, \alpha_2, \alpha_3)^T = (C_W, C_{FYI}, C_{MYI})^T$ is a 3×1 vector.

As n acts as the noise and modeling errors, to address problem (3) and find the optimal matching SICs, the least squares method is applied to undertake SIC estimation. The least squares method obtains a satisfactory estimation by minimizing the sum of the squares of the bias (noise) in the results. According to the characteristics of SIC, two constraints should be imposed on the least squares model: 1) the sum-to-one constraint, i.e., the sum of the proportion of each surface cover type in each pixel is equal to 1 ($\sum_{j=1}^3 \alpha_j = 1$); and 2) the nonnegative constraint, indicating that the SIC for each surface cover type should be a nonnegative value ($\alpha_j \geq 0$ for all $1 \leq j \leq 3$). To simultaneously satisfy the aforementioned two constraints, a least squares based method, i.e., FCLS [13], is utilized in this letter. FCLS is a linear-spectral-mixture-analysis-based method for material quantification, which can impose two constraints, namely, the abundance nonnegativity constraint and abundance sum-to-one constraint, simultaneously. According to the FCLS

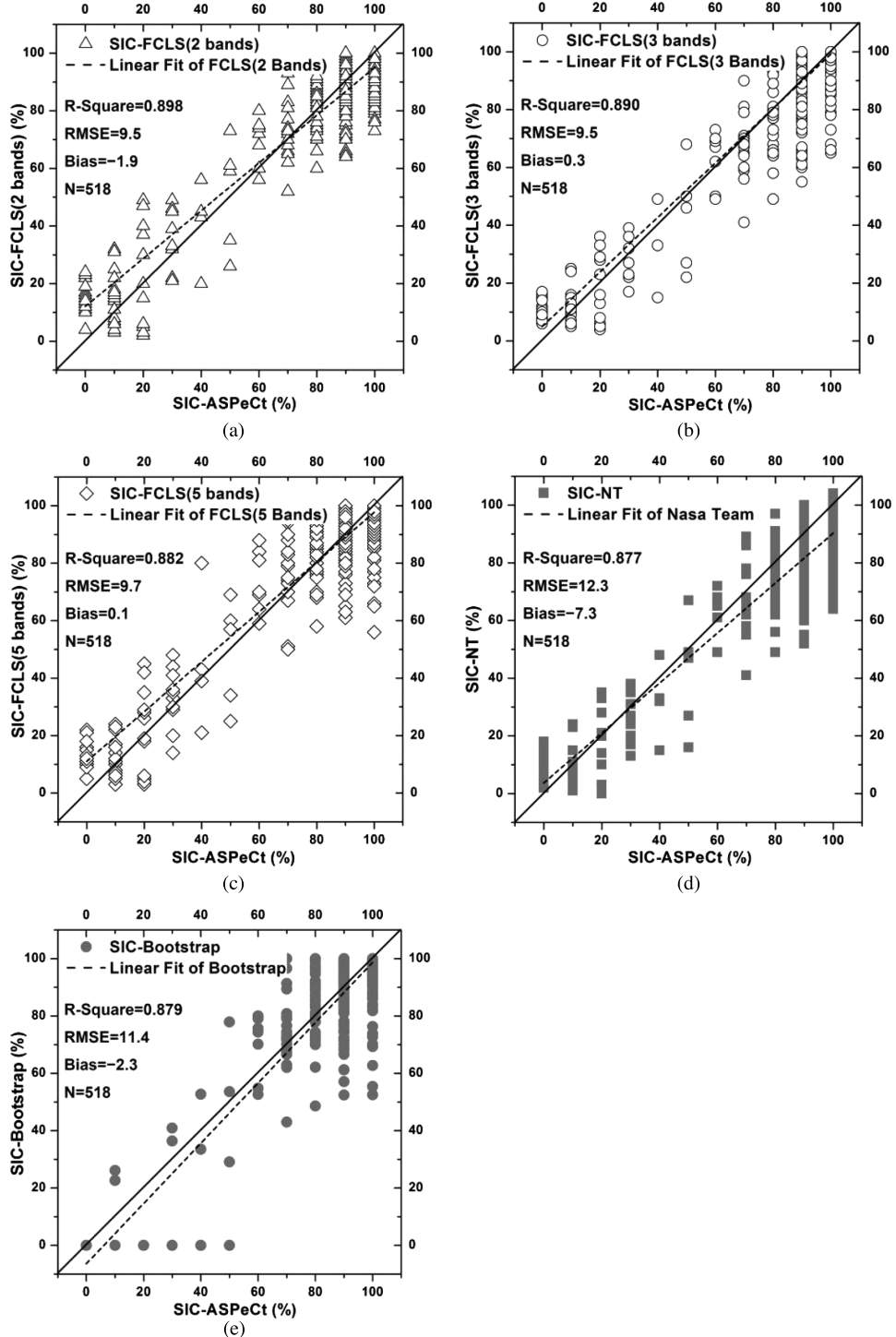


Fig. 2. Comparison between the total SIC results and the ASPeCt data ($N = 518$). (a) FCLS using two bands. (b) FCLS using three bands. (c) FCLS using five bands. (d) NT. (e) Bootstrap. The dotted line shows the regression result of each estimated total SIC result and ASPeCt data observation; the solid line indicates where the estimated total SICs would be equal to the ASPeCt data.

method, the optimization function of the SIC estimation can then be rewritten as

$$\min_{\alpha} \|\mathbf{T} - \mathbf{M}\alpha\|_F^2 \text{ s.t. } \alpha \geq \mathbf{0}, \mathbf{1}^T \alpha = 1 \quad (4)$$

where $\|\mathbf{X}\|_F = [\text{tr}(\mathbf{X}^T \mathbf{X})]^{1/2}$ represents the Frobenius norm of matrix \mathbf{X} , $\alpha \geq \mathbf{0}$ is equal to the nonnegative constraint, and $\mathbf{1}^T \alpha = 1$ represents the sum-to-one constraint.

B. Available Channels

The physical basis for distinguishing the three surface cover types is their differences in the different channels (e.g., frequencies and polarizations). Radiance ratios can minimize geophysical crosstalk [7] and make these differences more apparent [3]. Therefore, the polarization ratio (PR) and spectral gradient ratio (GR), respectively, are used to estimate the SIC in

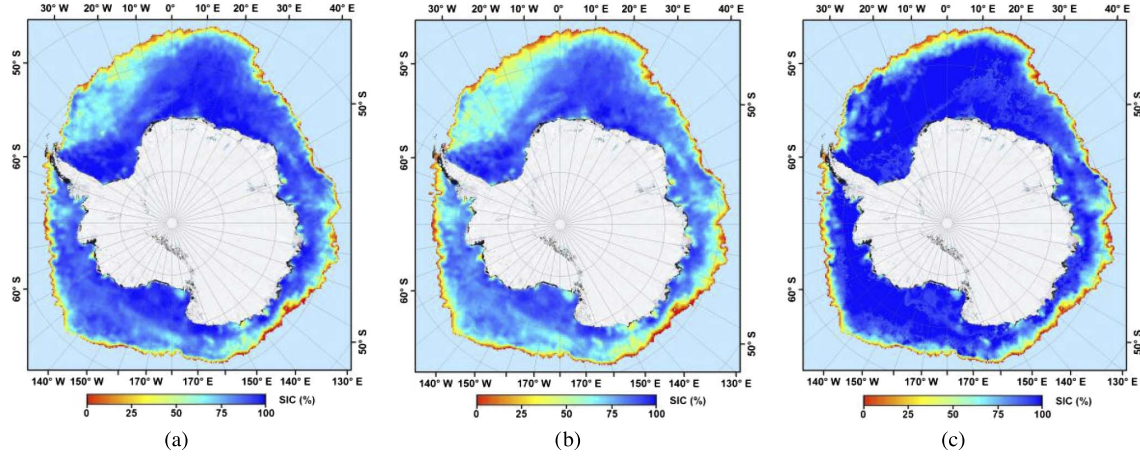


Fig. 3. Estimated SIC maps using each method. (a) FCLS using five bands. (b) NT. (c) Bootstrap.

combination with the original channels, as shown in the following equations:

$$\text{PR}(19) = \frac{[T_B(19V) - T_B(19H)]}{[T_B(19V) + T_B(19H)]} \quad (5)$$

$$\text{GR} \left(\frac{37V}{19V} \right) = \frac{[T_B(37V) - T_B(19V)]}{[T_B(37V) + T_B(19V)]} \quad (6)$$

where $T_B(V)$ is the BT for each GHz at the vertical polarization, and $T_B(H)$ is the BT for each GHz at the horizontal polarization. In this letter, three kinds of band combinations are used in the algorithm validation: 1) a two-band combination (only using the PR and GR); 2) a three-band combination (only using the original channels 19V, 19H, and 37V); and 3) a five-band combination (PR and GR combined with 19V, 19H, and 37V).

C. Tie Points

Tie points are a set of reference BTs representing the three different surface cover types (OW, FYI, and MYI). By specifying the tie points, T_{BW} , T_{BFYI} , and T_{BMYI} can be set as known values. Selection of an appropriate set of tie points is crucial for the proposed procedure. In this letter, the tie points (listed in Table II) from Comiso [6] are used.

IV. RESULTS AND ANALYSIS

The comparisons between the SSM/I-based SICs (the proposed method, the NT algorithm, and the bootstrap algorithm) and ASPeCt data were conducted from two aspects: total SIC and different surface cover type SICs. The relevant accuracy of each comparison was quantified in terms of mean bias, root-mean-square error (rmse), and determination coefficients (R-squared).

A. Total SIC Comparison

The total SIC is the ice concentration of each pixel, which is equal to the sum of C_{FYI} and C_{MYI} . This comparison was carried out between the total SICs from the proposed method

TABLE III
ACCURACY OF THE SSM/I-BASED SICs COMPARED WITH ASPeCt DATA IN SUMMER AND WINTER, RESPECTIVELY. THE TOTAL NUMBERS OF DATA OBSERVATIONS IN SUMMER AND WINTER WERE 169 AND 349, RESPECTIVELY

Method	Summer (N=169)		Winter (N=349)	
	Bias	RMSE	Bias	RMSE
FCLS (2 bands)	0.9	12.3	-3.2	7.7
FCLS (3 bands)	-3.2	12.2	2	7.9
FCLS (5 bands)	1.8	13.3	-0.7	7.4
NT	-5.8	13.2	-8	11.9
Bootstrap	-4.6	15.1	-1.4	9.1

TABLE IV
ACCURACY OF THE SSM/I-BASED SICs OF DIFFERENT ICE TYPES COMPARED WITH ASPeCt DATA ($N = 518$)

Method	FYI (N=518)		MYI (N=518)	
	Bias	RMSE	Bias	RMSE
FCLS (2 bands)	-4.6	18.4	2.8	16.1
FCLS (3 bands)	2.3	16.7	-2.1	15.3
FCLS (5 bands)	0.3	13.9	-0.2	11.0
NT	-10.1	22.1	2.9	18.0

(FCLS-based), the NT algorithm, and the bootstrap algorithm, and observations from the ASPeCt data set. For the *in situ* data, the pixels in the satellite image closest in time, and matching the geographic coordinates, were selected. The comparison results are presented in Fig. 2.

The results indicate that the proposed method with both two bands, three bands, and five bands is more accurate than the NT algorithm and the bootstrap algorithm. In comparison, the total SICs estimated by the proposed method using five bands show a lower bias, indicating that the estimated SICs are much closer to the actual observations. Maps of estimated results for each methods are shown in Fig. 3.

According to Andersen *et al.* [5], the accuracy values of SIC can be influenced by the seasonal (winter and summer) change due to the variations in the sea ice surface. Therefore, the accuracy values of the SIC in both summer and winter were generated, respectively (see Table III).

TABLE V
ACCURACY OF THE SSM/I-BASED SICs OF DIFFERENT ICE TYPES COMPARED WITH
ASPECT DATA IN SUMMER AND WINTER, RESPECTIVELY ($N = 518$)

Method	FYI				MYI			
	Summer (N=169)		Winter (N=349)		Summer (N=169)		Winter (N=349)	
	Bias	RMSE	Bias	RMSE	Bias	RMSE	Bias	RMSE
FCLS (2 bands)	-6.2	28.6	-3.8	10.4	7.2	26.4	0.6	6.8
FCLS (3 bands)	-0.5	25.4	3.7	10.1	-2.7	25.6	-1.7	5.5
FCLS (5 bands)	-0.7	20.6	0.8	9.1	2.5	17.6	-1.6	5.4
NT	-13.9	32.6	8.3	14.5	8.1	28.5	0.3	9.5

The results indicate that the proposed method consistently presents better accuracy values than the other methods. In Table III, the accuracy values of all the methods in summer are clearly lower than those in winter, among which the accuracy of the bootstrap-based SIC is the lowest. This is due to the fact that the ice consolidation in winter results in the values of the tie points and BT being stable. In contrast, this consolidation is easily destroyed by surface melt in summer. The bootstrap algorithm, which depends on the emissivity, is easily impacted by the fluctuations in the snow and ice surface temperature in summer. In contrast, the NT algorithm obtains higher accuracy since it utilizes the PR and GR, which are not sensitive to the discrepancies in the tie points coming from seasonal change [3], [7].

B. Comparison of SICs of Different Surface Cover Types

This comparison was carried out for the SICs of different surface cover types (MYI and FYI) between two-band-based FCLS, three-band-based FCLS, five-band-based FCLS, and the NT algorithm. The corresponding accuracy values are reported in Table IV.

In this comparison, the proposed method using five bands is more accurate than the two-band-based FCLS, the three-band-based FCLS, and the NT algorithm. This indicates that more channels can provide additional information to help distinguish multiple ice types, which is useful for estimating the SICs of multiple ice types. In contrast, the accuracy of FYI-SIC is lower than MYI-SIC. This phenomenon can be attributed to the presence of new ice, which is already known to be a problem for most of the SIC algorithms [4]. Compared with the results of the total SIC (see Fig. 2), the results in this comparison are worse. There are two factors that account for these results. One is the chosen tie point sets, and the other is the limited distribution of MYI in the Antarctic. The accuracy values of the SICs of multiple ice types in summer and winter were also generated (see Table V).

The proposed method also presents better accuracy values according to Table V. It can be seen that the results in winter are much more accurate than the results in summer, which is consistent with the results in Table III. Due to the absence of the nonnegative constraint of SIC, negative values (such as a total SIC of 63 with a corresponding FYI-SIC of 74 and a corresponding MYI-SIC of -11) frequently exist in the SICs of the different ice types estimated by the NT algorithm, which is abnormal in SIC estimation results.

V. CONCLUSION

In this letter, an effective SIC estimation procedure has been proposed by combining reformulation of the SIC estimation equation with the introduction of FCLS. The performance of the proposed method was found to be better than that of the NT algorithm and the bootstrap algorithm in quantitative comparisons. This letter demonstrates the benefit of incorporating numerical optimization into SIC estimation. Furthermore, the noise issue, in particular, should also be taken into consideration during the numerical optimization.

REFERENCES

- [1] J. C. Stroeve, T. Markus, L. Boisvert, J. Miller, and A. Barrett, "Changes in Arctic melt season and implications for sea ice loss," *Geophys. Res. Lett.*, vol. 41, no. 4, pp. 1216–1225, Feb. 2014.
- [2] J. C. Comiso and F. Nishio, "Trends in the sea ice cover using enhanced and compatible AMSR-E, SSM/I, and SMMR data," *J. Geophys. Res.-Oceans*, vol. 113, no. C2, 2008, Art ID. C02S07.
- [3] J. C. Comiso, D. J. Cavalieri, C. L. Parkinson, and P. Gloersen, "Passive microwave algorithms for sea ice concentration: A comparison of two techniques," *Remote Sens. Environ.*, vol. 60, no. 3, pp. 357–384, Jun. 1997.
- [4] N. Ivanova, O. M. Johannessen, L. T. Pedersen, and R. T. Tonboe, "Retrieval of arctic sea ice parameters by satellite passive microwave sensors: A comparison of eleven sea ice concentration algorithms," *IEEE Trans. Geosci. Remote Sens.*, vol. 52, no. 11, pp. 7233–7246, Nov. 2014.
- [5] S. Andersen, R. T. Tonboe, S. Kern, and H. Schyberg, "Improved retrieval of sea ice total concentration from spaceborne passive microwave observations using numerical weather prediction model fields: An inter-comparison of nine algorithms," *Remote Sens. Environ.*, vol. 104, no. 4, pp. 374–392, Oct. 2006.
- [6] J. C. Comiso, "Characteristics of arctic winter sea ice from satellite multispectral microwave observations," *J. Geophys. Res.*, vol. 91, no. C1, pp. 975–994, Jan. 1986.
- [7] D. J. Cavalieri, P. Gloersen, and W. J. Campbell, "Determination of sea ice parameters with the NIMBUS 7 SMMR," *J. Geophys. Res.*, vol. 89, no. D4, pp. 5355–5369, Jun. 1984.
- [8] R. O. Ramseier, "Sea ice validation," in *DMSP Special Sensor Microwave/Imager Calibration/Validation*, J. P. Hollinger, Ed. Washington, DC, USA: Naval Res. Lab., 1991.
- [9] L. Kaleschke *et al.*, "SSM/I sea ice remote sensing for mesoscale ocean-atmosphere interaction analysis," *Can. J. Remote Sens.*, vol. 27, no. 5, pp. 526–537, 2001.
- [10] T. Markus and D. J. Cavalieri, "An enhancement of the NASA Team sea ice algorithm," *IEEE Trans. Geosci. Remote Sens.*, vol. 38, no. 3, pp. 1387–1398, May 2000.
- [11] E. Svendsen, C. Matzler, and T. Grenfell, "A model for retrieving total sea ice concentration from a spaceborne dual-polarized passive microwave instrument operating near 90 GHz," *Int. J. Remote Sens.*, vol. 8, no. 10, pp. 1479–1487, Oct. 1987.
- [12] A. P. Worby *et al.*, "Thickness distribution of Antarctic sea ice," *J. Geophys. Res.-Oceans*, vol. 113, no. C5, 2008, Art ID. C05S92.
- [13] D. C. Heinz and C. Chang, "Fully constrained least squares linear spectral mixture analysis method for material quantification in hyperspectral imagery," *IEEE Trans. Geosci. Remote Sens.*, vol. 39, no. 3, pp. 529–545, Mar. 2001.